Available online at www.sciencedirect.com

ScienceDirect

IFAC Papers Online CONFERENCE PAPER ARCHIVE

IFAC PapersOnLine 58-9 (2024) 229–234

A Simple State-Space Model of Human Driver Applicable to Windy Conditions

Jakub Čelko * **Ondrej Mihálik** * **Michal Husák** *
Zdeněk Bradáč *

* *Department of Control and Instrumentation, Faculty of Electrical Engineering, Brno University of Technology, Brno, Czech republic, (e-mail: Jakub.Celko@vut.cz).*

Abstract: The paper is concerned with the design, verification and evaluation of a car-driving test scenario for human driver assessment. The scenario implemented in Unreal Engine adds four different wind characteristics which disturb the motion of a simulated vehicle. Besides, the driver is instructed to change the driving lane at defined intervals. These forcing functions enable the identification of the human-machine loop using state-space models. The parameters characterising the human dynamics are extracted from the model of the whole loop. As opposed to rather obsolete McRuer models, this approach follows the recent trends in the modelling of human-machine systems as multiloop systems or quadratically optimal controllers. Our results suggest that the model relying on a single transfer function with 4 parameters loses prediction capabilities during more realistic scenarios, in which random disturbances, such as wind gusts, affect the vehicle. In such cases, the multiloop model with the same number of parameters is able to capture human behaviour more accurately than McRuer model.

Keywords: driving simulator, human dynamics, identification, multiloop model

1. INTRODUCTION

Interaction between a driver and a vehicle represents an example of a human-machine system (HMS). Some of the first attempts to capture the dynamical behaviour of such HMS date back to the 1970s. One of these approaches was advanced by McRuer and Krendel (1974). It models the HMS as a simple feedback loop with two elements: the plant and the human controller, which are modelled using transfer functions $S(s)$ and $R(s)$, respectively. Another prominent approach employs a multiloop representation and the human is modelled as a static state feedback controller followed by pure delays, Donges (1978). These approaches were subsequently combined and extended in various forms and modifications, Hess (1980).

Recent views on the HMS and their modelling in general are set out in, for example, sources Macadam (2003); Xu et al. (2017); Kolarik and Slanina (2017). Various methods of monitoring humans by recording their signals were proposed by Mulder et al. (2018); Noubissie Tientcheu et al. (2022); Otahalova et al. (2012). According to these studies, the most popular modelling methods can be classified into:

- artificial neural networks (ANN),
- hidden Markov models (HMM),
- feedback control theory approach.

In our paper, we focus on the control theory approach. This decision is motivated by the bulk of recent literature in this modelling stream.

The paper is divided as follows. In Section 2 we discuss some of the most popular models of human driver. Our experimental setup and data acquisition are described in Section 3. Section 4 specifies the chosen identification method and structure of identified driver models. Section 5 presents the parameters of the identified models and compares the multiloop models with transfer function models. It is shown that the transfer function model is applicable only when wind is absent or very small. In contrast, the multiloop approach offers very good predictions even during scenarios with the strongest disturbances.

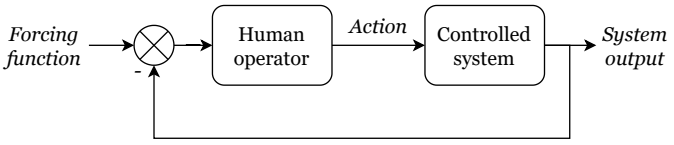

Fig. 1. Simple feedback loop, modeling human using a single transfer function.

2. RELATED WORK

McRuer model is often used only as a simple feedback controller (Fig. 1). Drivers were modelled using 2nd order transfer function by Michalík et al. (2021).

However, real-world drivers often learn optimal inputs into the system, especially during repetitive tasks, as described in Rasmussen (1983). As the driver becomes skilled, these learned optimal input waveforms may be modelled using a feedforward controller. Simple feedback also has limited degrees of freedom; therefore, state feedback models are more common. One of the first occurrences of state feedback driver models in literature was published by Donges (1978), where a two-level model of driver steering

10.1016/j.ifacol.2024.07.401

behaviour is presented. The model combines anticipatory open-loop control forced by road curvature shown to the driver in advance; and a compensatory feedback layer where the errors from the plant's individual states are multiplied by static gains followed by pure delays. Similar multiloop models were later brought into prominence by Mulder et al. (2018); Nash and Cole (2020, 2022a), who enhanced linear models with non-linearities and model predictive control (MPC).

3. VEHICLE DRIVING SIMULATOR

The research took advantage of an already existing vehicle driving simulator (VDS) developed and described by Michalík et al. (2021). A screenshot from the measurement can be seen in Fig. 3. Apart from the lane change forcing function, there were no other disturbance signals. Therefore, several changes had to be made in the Unreal Engine framework, in which the VDS is implemented.

We proposed adding a new disturbance signal, which could mimic the wind and wind gusts affecting the motion of the vehicle and altering its direction of travel. Generated disturbance signal $v(nT_s)$ is added to the drivers' action input, directly affecting the front wheels of the car, which represents a disturbance signal at the input of the controlled plant. We believe that the addition of this new input signal will help to improve the quality of identified models.

Disturbance generators can be configured: the experimenter can choose between the *White Noise* generator and the *Pseudo Random Binary Sequence* (PRBS) generator. After a few experiments, it was obvious that disturbance signals taken as raw outputs from these generators are not suitable, because of their broad frequency content. High-frequency components of the noise were affecting the motion of the vehicle too fast for humans to react. The low-frequency content of the PRBS created a significant mean value resulting in an unnatural, continuous yaw of the steering wheel.

To solve the aforementioned problems, three different filters inserted after the disturbance signal generator were created. The experimenter can choose from four options stated in Table 1, only one option at a time. The 4th order filter is implemented with configurable time constant T_f. Magnitude frequency responses of the filters are shown in Fig. 2, 4th order filter is plotted for $T_f = 1$ s. Examples of the disturbance signals can be found in Figs. 4 and 5.

Table 1. Disturbance signal filters

Filter name	$F(s)$	$H(z)$
No Filter	1	1
1st Order	$\frac{s}{5s+1}$	$\frac{0.2(1-z^{-1})}{1-0.998z^{-1}}$
2nd Order	$\frac{s}{(s+1)^2}$	$\frac{0.0099(1-z^{-1})}{(1-0.99z^{-1})^2}$
4th Order	$\frac{(T_f s)^2}{(T_f s+1)^4}$	$\frac{K_f(1+b_f z^{-1})(1-z^{-1})^2}{(1-a_f z^{-1})^4}$

To successfully analyze the HMS the logging function records: the timestamps of the samples, the disturbance signal, control error (difference between the centre of the desired line and actual car position on the road), driver's action (angle of the steering wheel) and vehicle speed.

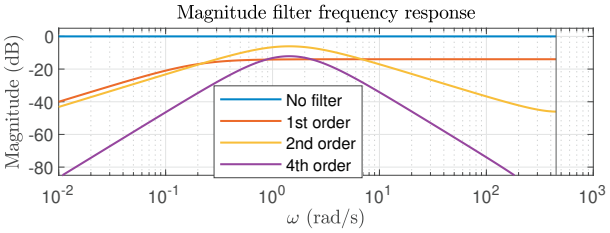

Fig. 2. Magnitude frequency responses of the noise filters applied during test scenarios.

Fig. 3. VDS screenshot showing a typical test scenario.

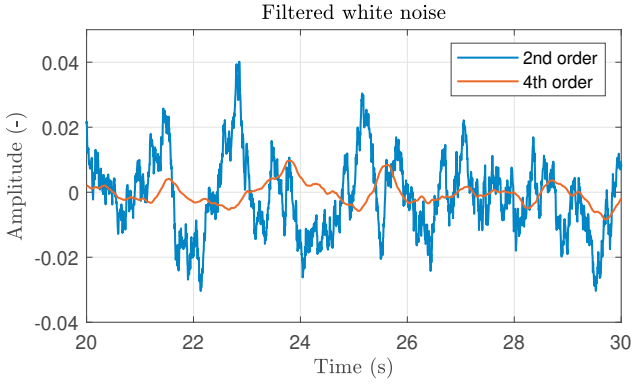

Fig. 4. Filtered white noise simulating effects of wind

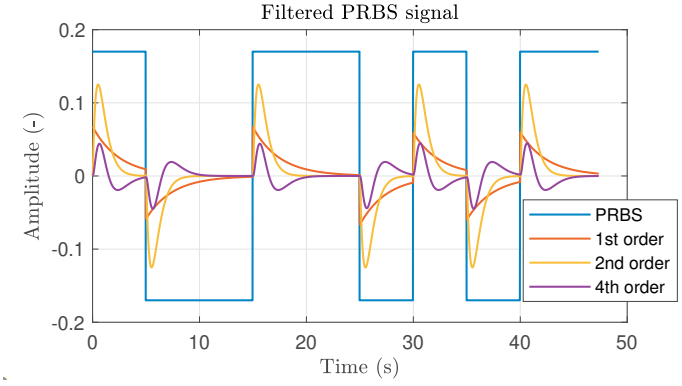

Fig. 5. Filtered PRBS signal

4. DRIVER MODEL IDENTIFICATION

Driver model obtained with a direct identification approach based only on measured control error and steering

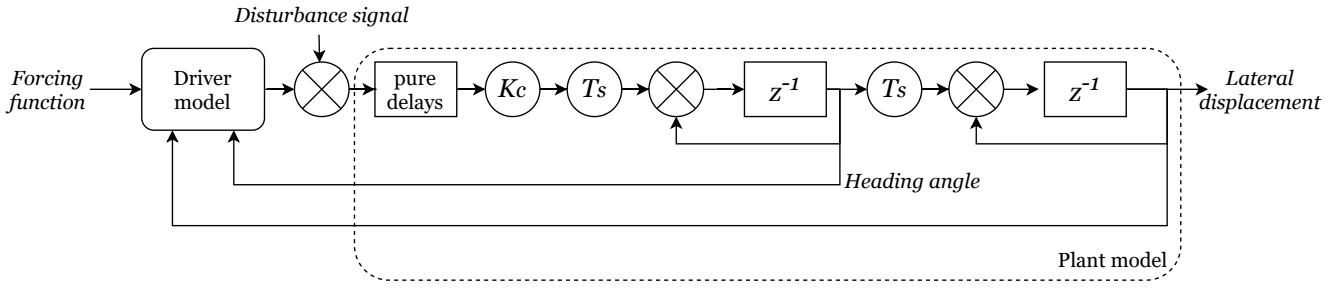

Fig. 6. Closed loop model with details of the vehicle dynamics model.

wheel angle may be likely biased to the inverse of the controlled plant's dynamics in cases when the control error signal is close to zero on long time intervals thus the human driver only injects his significant random noise to the loop. This is discussed in detail by Nash and Cole (2020); Ljung (1999).

Therefore, the indirect identification method was used, identifying the driver model in a closed loop together with known vehicle dynamics (Fig. 6), all described by a discrete state-space model. The model has two inputs (desired lane forcing function and disturbance signal) and two outputs (control error and steering wheel angle signal). MATLAB function `ssest` was used to find optimal model parameters to fit measured data. Function input parameters are: input and output signals and closed-loop system structure with specification which coefficients are identified (driver's model) and which are fixed (all other coefficients including vehicle dynamics).

Vehicle gain is $K_\mathrm{c} = 73$ and vehicle model also has a delay of 40 steps, which is caused by the implementation of the given VDS. The sampling period $T_\mathrm{S} \approx 0.07$ ms was calculated as the mean difference of samples' timestamps. This was necessary because the VDS causes a slight sampling non-uniformity.

The `ssest` function does not allow identification of driver's delay simply as a parameter. The delay must be specified in the state-space matrix as a line of one-step delays in series. For each set of data, numerous models were identified with linearly increasing delays and the model with the highest model efficiency (ME) was selected. This measure of model quality is computed using the equation

$$\mathrm{ME}_\mathrm{train} = 1 - \frac{\sum_{n=0}^{N-1}[\hat{x}(nT_\mathrm{s}) - x(nT_\mathrm{s})]^2}{\sum_{n=0}^{N-1}\left[x(nT_\mathrm{s}) - \overline{x}\right]^2}, \qquad (1)$$

where $x(nT_\mathrm{s})$ is the training data, $\overline{x}$ is their mean value, and $\hat{x}(nT_\mathrm{s})$ is for the prediction of the model. In MATLAB, Ljung (2022), a similar quantity is referred to as "fit", but the fraction in (3) is subjected to square root. Hence $\mathrm{ME}_\mathrm{train} = 1-(1-\mathrm{fit})^2$. Since there are two output signals for which MEs are evaluated, the mean value from both MEs was used for model selection.

In this paper, two driver models are compared. Both models have 3 parameters plus delay, τ. A first-order Donges (1978) model is shown in Fig. 7. It takes feedback from individual states of the vehicle. A first-order filter was added to the lateral displacement feedback loop as a human reaction to step change in the forcing function can not be modelled using a static gain.

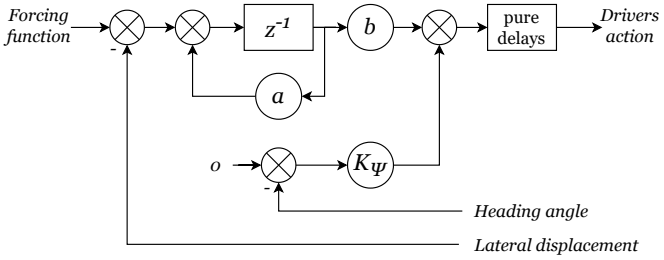

Fig. 7. First-order Donges model.

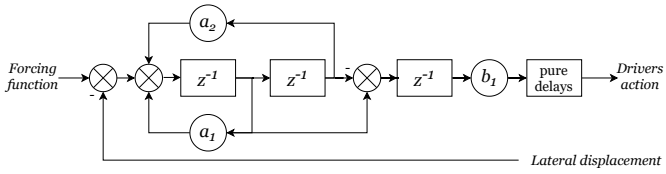

Fig. 8. 2nd-order McRuer model.

A 2nd-order McRuer model proposed by Michalík et al. (2021) is shown in Fig. 8. It takes feedback only from the plant's output (lateral displacement). Assuming zero-order hold (ZOH) equivalent, the discrete model can be converted back to continuous

$$F_\mathrm{R}(s) = \frac{K_\mathrm{R} s}{T_\mathrm{R}^2 s^2 + 2\xi T_\mathrm{R} s + 1} \mathrm{e}^{-\tau s}, \qquad (2)$$

whose parameters are described in the original article. Models were identified from measured data from 12 tested drivers. All measurements were taken with a constant vehicle speed of 90 km/h. Each driver was measured in four different scenarios with various disturbance signals whose numbers were assigned as follows:

(1) Measurement with no noise;
(2) Measurement with noise coloured by 4th order filter with $T_\mathrm{f} = 1$ s;
(3) Measurement with noise coloured by 2nd order filter;
(4) Measurement with PRBS coloured by 4th order filter with $T_\mathrm{f} = 2$ s.

5. ASSESSMENT OF IDENTIFIED MODELS

To quantify the prediction capabilities of investigated models, we use the standard cross-validation process, see Hastie (2009), which divides data into K folds. We use $K = 2$ folds: $x_1(nT_\mathrm{s})$ and $x_2(nT_\mathrm{s})$. It is worth mentioning that the first two lane-change steps were removed from every measurement (before the folds creation), as the vehicle was still accelerating to reach the desired speed

and therefore the vehicle's dynamics were changing. We train two models:

(1) The first model is trained using fold $x_1(nT_\mathrm{s})$ and validated using the fold $x_2(nT_\mathrm{s})$.
(2) The second model is trained using the fold $x_2(nT_\mathrm{s})$ and validated using the fold $x_1(nT_\mathrm{s})$.

This ensures that the performance of the model is tested on data that differs from the training data. ME on the validation fold is defined as

$$\mathrm{ME}_\mathrm{val} = 1 - \frac{\sum_{n=0}^{N-1}[\hat{x}_k(nT_\mathrm{s}) - x_k(nT_\mathrm{s})]^2}{\sum_{n=0}^{N-1}\left[x_k(nT_\mathrm{s}) - \overline{x}_k\right]^2}, \quad k = 1, 2. \quad (3)$$

Here $x_k(nT_\mathrm{s})$ is the validation signal and $\hat{x}_k(nT_\mathrm{s})$ is the signal predicted by the model. The ME is clearly related to the mean squared error (MSE), which is proportional to the term in the nominator of (3). Higher ME values indicate better prediction capabilities of the model. The limiting value ME $= 1$ is attained only when the model prediction is identical to the validation data.

As can be seen in Fig. 9, the performance of both models generally declines with stronger disturbance signals. However, the Donges model was able to approximate measured data quite well even in scenarios with the strongest disturbances while the identification function could not find any sufficient 2nd order McRuer model in scenarios 3 and 4. In fact, for Scenario 4, the identified model degraded into a form which has no continuous equivalent. For that reason, the first-order McRuer model was also identified for this scenario but no significant improvements in model MEs were observed.

Identified parameters of the first-order Donges model for each driver and scenario are shown in Fig. 10. For easier interpretation the discrete first-order model with coefficients a and b was transformed, assuming ZOH, to its continuous-time equivalent with time constant T and static gain K_Y, reading

$$F_\mathrm{discr}(z) = \frac{b}{z-a} \quad \Longleftrightarrow \quad F_\mathrm{cont}(s) = \frac{K_\mathrm{Y}}{Ts+1}. \quad (4)$$

Fig. 10 indicates that model gains K_Y and K_Ψ tend to increase with the increasing disturbance signal. This finding is in accordance with Nash and Cole (2022b) and might suggest that the driver needs stronger action to compensate the disturbance. The filter time constant T remains approximately the same in the first three scenarios but the last scenario indicates a noticeable increase in T. This could be related to the type of disturbance signal; random signal of coloured noise in Scenarios 2 and 3 does not affect this parameter while filtered PRBS is predictable, therefore drivers can adapt their behaviour accordingly. On the other hand, driver transport delays are decreasing significantly as the disturbance signal increases. Possible explanation could be either that the driver gets bored or tired when nothing happens in the scenario for a long period of time and therefore his reaction to line change is slower; or with strong disturbance signal resulting in continuous steering wheel angle changes (see Figs. 12, 13, and 14) it might be difficult to differentiate between pure delays and driver dynamics. Thus a decrease in the delay τ may be compensated by an increase in time constant T, and vice versa.

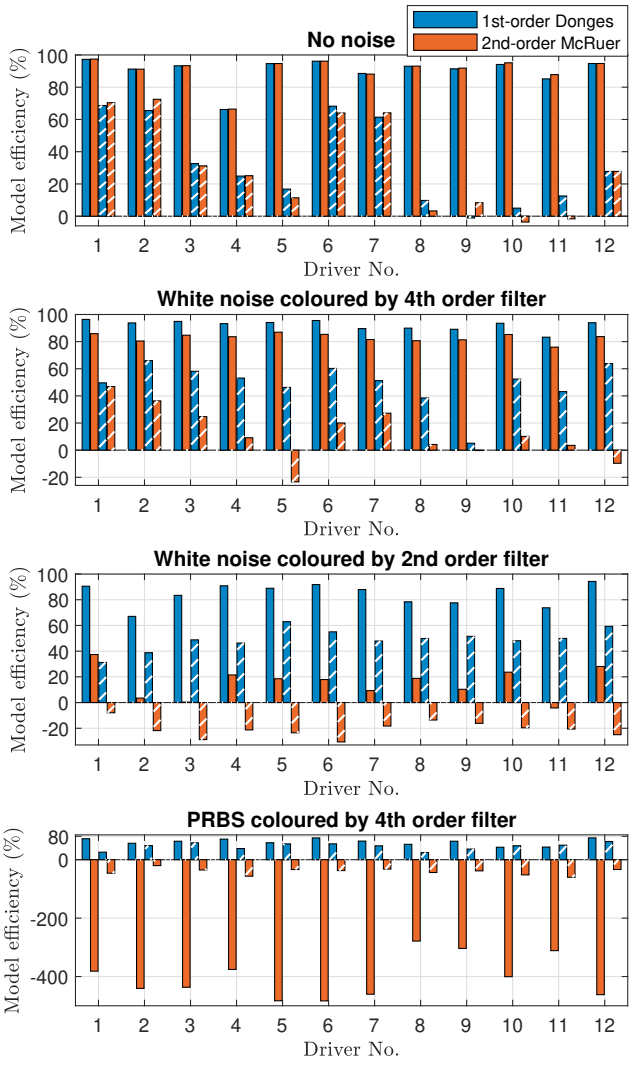

Fig. 9. Model efficiency on validation data during four different scenarios. Plain bars correspond to MEs of the control error signal; hatched bars to MEs of the steering wheel angle signal.

Parameter values of the McRuer model are shown in Fig. 11. Note, however, that for Scenario 4 and for the last driver in Scenario 3, first-order McRuer model parameters are plotted as there was no continuous equivalent for the second-order McRuer model. Therefore the damping ξ is zero and the time constant T_R has a different meaning than in the first 3 scenarios (except driver 12 in Scenario 3).

In Figs. 12, 13 and 14 a comparison between measured data and analysed models is shown for selected time periods. Figs. 12 and 13 show that the McRuer model is insensitive to the disturbances entering the loop, unable to model drivers' actions in compensating the error signal. In Fig. 14 a first-order McRuer model is plotted, as analysed 2nd order McRuer model degraded to a first-order filter. Furthermore, this model's prediction of the control error is completely unusable in the last scenario.

In contrast to the McRuer model, the first-order Donges model approximates drivers' actions very well in the first three scenarios, covering not only the lane change actions but also drivers reactions to the disturbances entering the

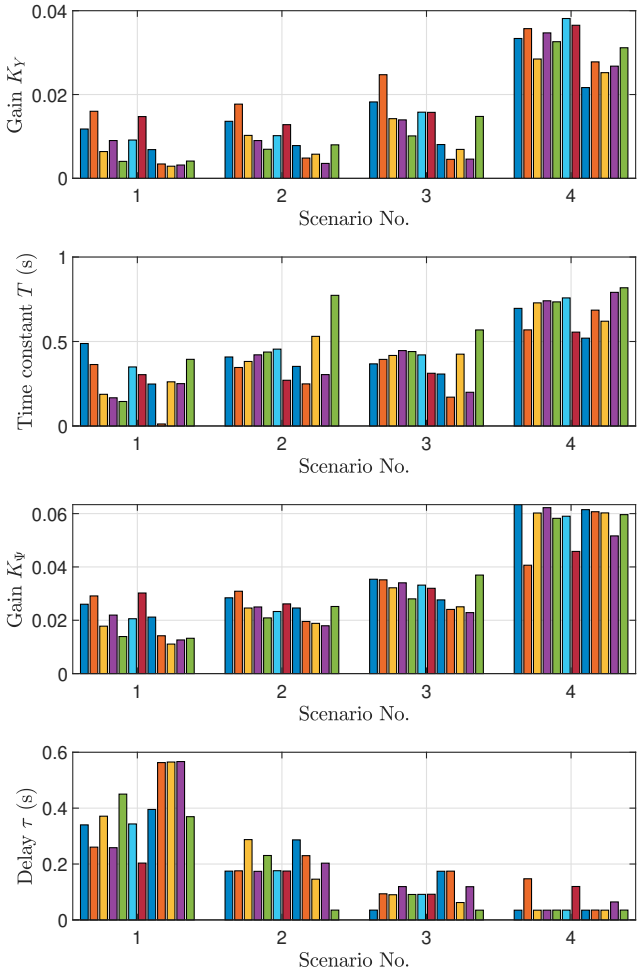

Fig. 10. Identified parameter values for the first-order Donges model.

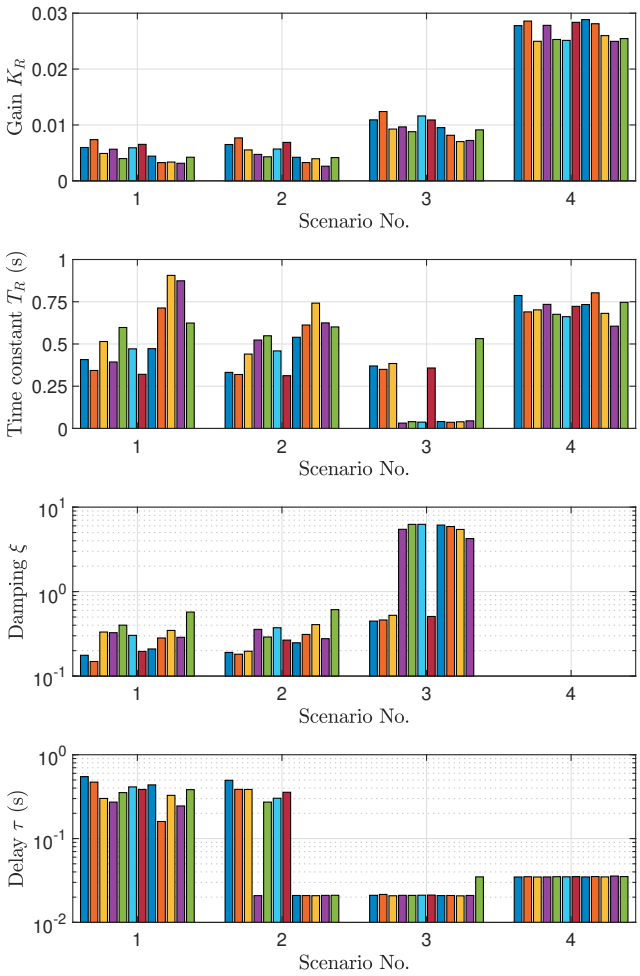

Fig. 11. Identified parameter values for McRuer models. Scenarios 1–3 use a 2nd order model (2), except for the driver 12 in scenario 3. This driver and scenario 4 rely on the first-order model.

loop. Model performance in Scenario 4 is decent; despite being significantly worse than in the first three scenarios, it still can represent at least the main drivers actions.

6. CONCLUSION

In this paper, we extended existing VDS and presented new scenarios which are useful for the identification of a HMS model. We pointed out the disadvantages of feedback models relying on a single feedback transfer function controller and provided a multiloop state-space model which is in accordance with the recent advancements in the field of HMS models. The 2nd-order McRuer feedback model is incapable to cope with wind disturbances which enter the feedback HMS. Hence, the larger the disturbance, the worse the prediction of such model. The model cannot predict the behaviour of the loop during scenarios with the strongest disturbances (scenarios 3 and 4).

The first-order Donges model outperforms the McRuer model in all scenarios with disturbances and has virtually the same ME when the disturbances are excluded. Therefore, we recommended to fully focus on multiloop models in future research. Further data collection and analysis will be needed to better explain the changes in identified model parameters and the effect of various input signals. This could clarify the reason and principles of the above-mentioned parameter changes.

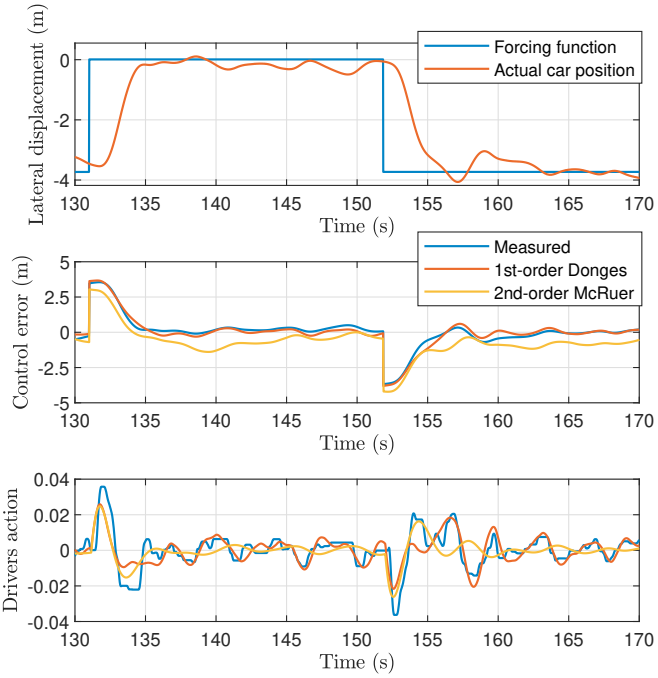

Fig. 12. Validation data and predicted signal waveforms during scenario 2.

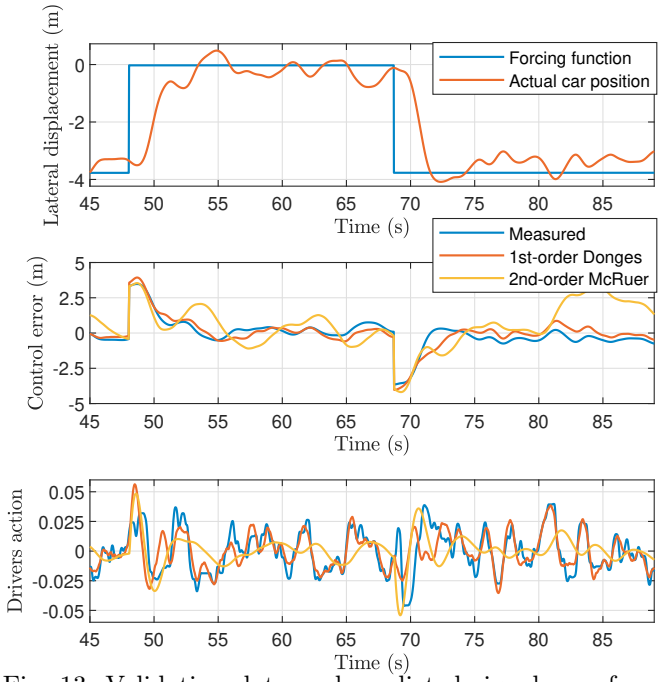

Fig. 13. Validation data and predicted signal waveforms during scenario 3.

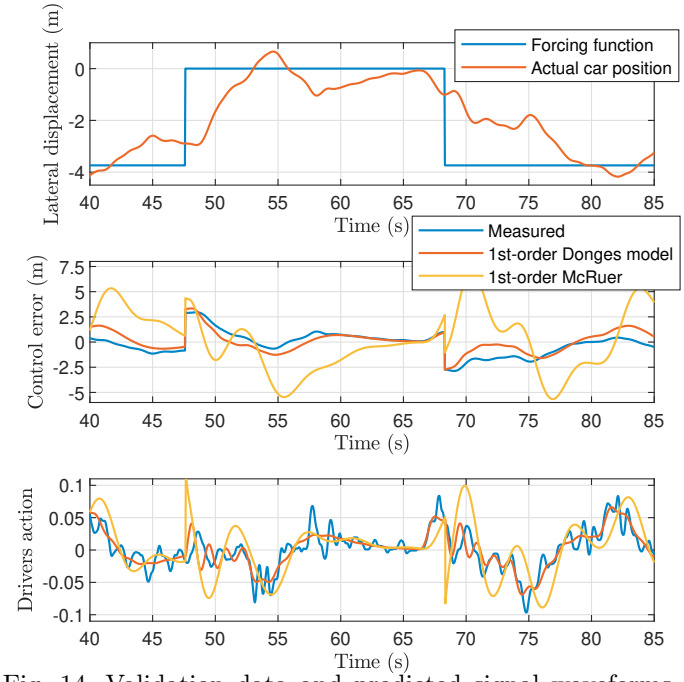

Fig. 14. Validation data and predicted signal waveforms during scenario 4.

ACKNOWLEDGEMENTS

The completion of this paper was made possible by the grant No. FEKT-S-23-8451—"Research on advanced methods and technologies in cybernetics, robotics, artificial intelligence, automation and measurement" financially supported by the Internal science fund of Brno University of Technology.

REFERENCES

Donges, E. (1978). A two-level model of driver steering behavior. *Human factors*, 20(6), 691–707.

Hastie, T. (2009). *The elements of statistical learning: data mining, inference, and prediction*, chapter 7, Model assessment and selection, 219–259. Springer series in statistics. Springer, New York, 2nd ed. edition.

Hess, R. (1980). Structural model of the adaptive human pilot. *Journal of guidance and control*, 3(5), 416–423.

Kolarik, J. and Slanina, Z. (2017). Fuzzy control application in swarm robotics cars. In *2017 18th International Carpathian Control Conference (ICCC)*, 327–331. doi: 10.1109/CarpathianCC.2017.7970420.

Ljung, L. (1999). *System identification : theory for the user*. Prentice Hall PTR, Upper Saddle River, 2nd ed. edition.

Ljung, L. (2022). *System Identification Toolbox: Reference*. MathWorks, Natick, (MA). URL `https://www.mathworks.com/help/pdf_doc/ident/ident_ref.pdf`.

Macadam, C.C. (2003). Understanding and modeling the human driver. *Vehicle System Dynamics*, 40(1-3), 101–134. doi:10.1076/vesd.40.1.101.15875.

McRuer, D.T. and Krendel, E.S. (1974). *Mathematical Models of Human Pilot Behavior*. AGARD, London.

Michalík, D., Jirgl, M., Arm, J., and Fiedler, P. (2021). Developing an unreal engine 4-based vehicle driving simulator applicable in driver behavior analysis—a technical perspective. *Safety*, 7(2). doi:10.3390/safety7020025. URL `https://www.mdpi.com/2313-576X/7/2/25`.

Mulder, M., Pool, D.M., Abbink, D.A., Boer, E.R., Zaal, P.M.T., Drop, F.M., van der El, K., and van Paassen, M.M. (2018). Manual control cybernetics: State-of-the-art and current trends. *IEEE transactions on human-machine systems*, 48(5), 468–485.

Nash, C.J. and Cole, D.J. (2020). Identification and validation of a driver steering control model incorporating human sensory dynamics. *Vehicle system dynamics*, 58(4), 495–517.

Nash, C.J. and Cole, D.J. (2022a). Identification of a driver model incorporating sensory dynamics, with nonlinear vehicle dynamics and transient disturbances. *Vehicle system dynamics*, 60(8), 2805–2824.

Nash, C.J. and Cole, D.J. (2022b). A simulation study of human sensory dynamics and driver–vehicle response. *Journal of dynamic systems, measurement, and control*, 144(6).

Noubissie Tientcheu, S.I., Du, S., and Djouani, K. (2022). Review on haptic assistive driving systems based on drivers' steering-wheel operating behaviour. *Electronics (Basel)*, 11(13), 2102.

Otahalova, T., Slanina, Z., and Vala, D. (2012). Embedded sensors system for real time biomedical data acquisition and analysis. In *2012 11th International Conference on Programmable Devices and Embedded Systems*, volume 45, 261–264. doi: https://doi.org/10.3182/20120523-3-CZ-3015.00050.

Rasmussen, J. (1983). Skills, rules, and knowledge; signals, signs, and symbols, and other distinctions in human performance models. *IEEE Transactions on Systems, Man, and Cybernetics*, SMC-13(3), 257–266. doi: 10.1109/TSMC.1983.6313160.

Xu, S., Tan, W., Efremov, A.V., Sun, L., and Qu, X. (2017). Review of control models for human pilot behavior. *Annual Reviews in Control*, 44, 274–291.